Research Square

Preprints are preliminary reports that have not undergone peer review.
They should not be considered conclusive, used to inform clinical practice,
or referenced by the media as validated information.

Uncertainty-aware overturning stability and operating boundaries of a compact transport vehicle-mounted crane boom

Wei Ding
State Grid Yancheng Power Supply Company
Qiang Zhang
State Grid Yancheng Power Supply Company
Yunfeng Dai
lyzzjdx12@163.com

State Grid Yancheng Power Supply Company
Feng Zhao
State Grid Yancheng Power Supply Company
Hongmei Cui
State Grid Yancheng Power Supply Company
Yihua Wang
State Grid Yancheng Power Supply Company

Article

Keywords: compact mobile crane, transport vehicle, overturning stability, support edge, slope, wind load, uncertainty propagation

Posted Date: October 12th, 2026

DOI: https://doi.org/10.21203/rs.3.rs-10654912/v1

License: This work is licensed under a Creative Commons Attribution 4.0 International License.
Read Full License

Additional Declarations: No competing interests reported.

Version of Record: A version of this preprint was published at Scientific Reports on November 4th, 2026. See the published version at https://doi.org/10.1038/s41598-026-78622-y.

Uncertainty-aware overturning stability and operating boundaries of a compact transport vehicle-mounted crane boom

Wei Ding[1], Qiang Zhang[1], Yunfeng Dai[1*], Feng Zhao[1], Hongmei Cui[1] , Yihua Wang[1]

State Grid Yancheng Power Supply Company, Yancheng 224000, Jiangsu, China

*Correspondence: Yunfeng Dai ,lyzzjdx12@163.com

Abstract

Compact material carriers equipped with crane booms can reduce manual handling at transmission-line construction sites, but the coupled lifting vehicle has overturning resistance that changes with support mode, slope, turning acceleration, boom orientation and wind. This study formulates a support-edge moment model for seven governing states: non-working wind, empty and loaded longitudinal travel, empty and loaded lateral turning, and two limiting lift orientations. Deterministic boundary sweeps are followed by 10,000 fixed-seed uncertainty evaluations per state. The baseline stability factor K is 2.67 for non-working wind, 1.06 and 3.61 for empty and loaded longitudinal travel, 1.29 and 1.25 for empty and loaded lateral turning, and 1.03 for both limiting lift orientations after working-wind moment is included. The empty longitudinal case reaches K = 1 near 15.5°, supporting a conservative 15° travel limit. At a 15° cross-slope and 5 m turning radius, the critical speeds are approximately 3.4 m s−1, so a 3 m s−1 operating point provides only a moderate reserve. For a 1.5 m wind-force height and 150 N m−2 pressure, the critical projected boom areas are 1.65–1.66 m² and change strongly with force height. Uncertainty analysis identifies the empty longitudinal and lifting states as the least robust. These computational screening results define measurable validation targets and configuration-specific controls for subsequent certification testing.

Keywords: compact mobile crane; transport vehicle; overturning stability; support edge; slope; wind load; uncertainty propagation

Introduction

Overhead transmission-line construction frequently takes place beyond paved roads. Access routes may be narrow, weak, muddy or steep, and the final work position can be separated from a serviceable road by agricultural land or temporary tracks. Large trucks and truck cranes therefore cannot always deliver sand, tower members, fittings and construction tools directly to the point of use. Small tyre- or track-based carriers offer better manoeuvrability and lower ground pressure, but repeated transfer from the carrier to the work position reduces productivity and increases manual handling. Mounting a compact crane boom on the carrier appears to solve that logistical problem. Mechanically, however, the modification converts a low-speed transporter into a lifting system whose centre of gravity and external moment change continuously.

Conventional capacity labels are insufficient for such a machine. A lifted mass creates different overturning effects when the boom is retracted or extended, aligned with the vehicle or slewed toward a side, stationary or accelerating, sheltered or exposed to wind. The relevant support boundary also changes. During travel, the potential tipping axes join adjacent wheel contact regions; during lifting, fully deployed outriggers can enlarge the support polygon. Computer-aided rotary-crane assessment has shown why the instantaneous configuration should be evaluated rather than represented by a single nominal capacity [1]. Wind-wise selection research likewise demonstrates that crane geometry and environmental loading must be treated together [2]. The same principle appears in rough-terrain mobile manipulation, where stability constraints are incorporated into trajectory planning [3] and analytical supporting-force solutions use loss of positive contact reaction as a direct physical indicator of impending tip-over [4].

The boom and carrier cannot be analysed independently. Configuration-selection research shows that different arm postures transmit different wrenches to a mobile base even when the payload and end-effector speed are unchanged [5]. Mobile-crane positioning accuracy is also affected by the sequential movement of crane joints and structural compliance [6]. For a field machine, these kinematic effects occur on terrain whose level may

be uncertain. Road-level identification for all-terrain cranes provides a route to estimating that disturbance [7], while coordinated position-force levelling has been proposed to reduce platform attitude error and reaction imbalance [8]. These studies support a formulation that evaluates every candidate tipping edge and treats platform inclination as a measured state rather than a negligible installation detail.

Wind adds a second configuration-dependent action. Numerical and analytical investigation of tower-crane overturning shows that critical wind speed varies with both wind direction and crane configuration [9]. Load sway can further amplify the response of a mobile crane subjected to wind [10]. Digital-twin lift planning increasingly combines crane location, capacity and spatial constraints before execution [11]. Although the present carrier is smaller than a tower or large mobile crane, the governing mechanics are the same: wind force is proportional to pressure, aerodynamic coefficient and projected area, whereas overturning moment also depends on the effective height of that force. A statement that an exposed area is safe or unsafe is therefore incomplete without pressure and force height.

Compact construction carriers also share characteristics with agricultural and off-road vehicles: narrow track, low-speed operation, irregular terrain and an elevated or movable load. A recent review of tractor rollover and stability control identifies centre-of-gravity height, speed, slope and active control as interacting determinants [12]. Validated multibody work shows that chassis torsional flexibility can alter rollover threshold [13]. Multidimensional vehicle simulations similarly demonstrate coupled effects of speed, centre-of-gravity height and steering input [14]. Pavement roughness and differential settlement reduce available rollover or skidding margins even when the nominal road grade is unchanged [15]. Consequently, a rigid-body static calculation is useful for screening but should not be mistaken for a complete prediction of field behaviour.

Whole-machine stability of a compact crane carrier requires more than isolated load calculations. Non-working wind, travel and lifting states use different support polygons and different combinations of self-weight, inertia, payload and aerodynamic force. A journal-level assessment must therefore use consistent symbols and units, combine forces about the active tipping edge, include working wind in lifting moments, and evaluate how operating limits change when uncertain geometry and environmental inputs vary.

This study asks a focused and testable question: how robust are the operating boundaries when force and lever-arm data are expressed in one support-edge framework and varied over plausible engineering ranges? The analysis introduces a stability factor and a normalised reserve, calculates baseline moments, sweeps slope, turning speed, radius, wind pressure and projected area, and propagates uncertainty through 10,000 fixed-seed evaluations for each governing state.

The contribution is a reproducible screening method rather than a new certification standard. Modern tip-over avoidance for mobile manipulators uses dynamic stability measures and active reconfiguration [16], and experimental work on small-footprint systems demonstrates the value of detecting instability before support is lost [17]. Uneven-terrain end-effector control further shows that robust feedback is needed when disturbance cannot be modelled exactly [18]. The calculations here identify which quantities such a sensing and control system must measure, which configurations require the greatest reserve and which prototype tests should be prioritised. They do not replace structural design, ground-bearing assessment, hydraulic validation or controlled physical testing.

System definition and modelling framework

Support modes and tipping lines

The machine combines a compact wheeled chassis, a crane-boom assembly with its own support legs and rear outriggers. The analysis assumes that the chassis, boom and outrigger structures satisfy their local strength requirements; the scope is whole-machine overturning. In travel and non-working states, tipping lines connect wheel centres (Fig. 1). In the lifting state, tipping lines connect the deployed support centres (Fig. 2). Outrigger support is credited only when the outriggers are deployed.

Figures 1 and 2 define the wheel-supported and outrigger-supported tipping geometries. The support-edge formulation evaluates each candidate state about the edge that gives the smallest signed moment. This

approach is compatible with supporting-force analysis for mobile manipulators [4] and analytic treatment of variable-span truck-crane outriggers [23].

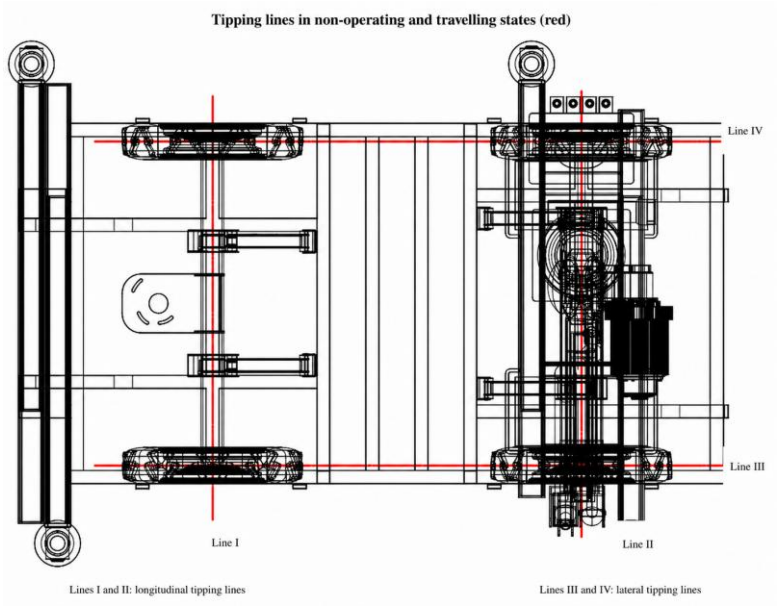


Figure 1. Wheel-supported tipping-line geometry. The red lines connect wheel centres and define the candidate longitudinal and lateral tipping axes for non-working and travel states.

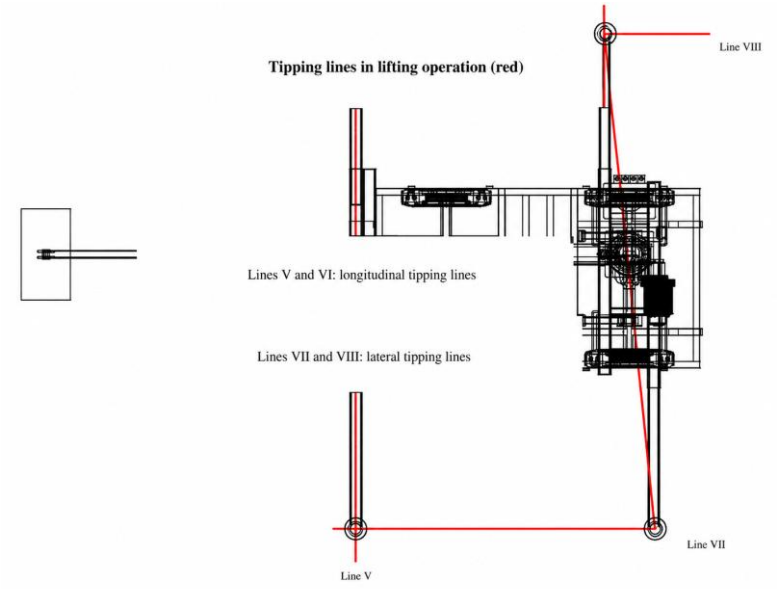


Figure 2. Outrigger-supported tipping-line geometry. The deployed support centres define the candidate tipping axes during lifting.

Standard load combinations

Tables 1–3 define the calculation loads, wind-affected actions and mechanism increase coefficients. The machine is assigned to mechanism class M6, giving $\gamma n = 1.20$. These normative inputs are used consistently in all baseline scenarios and parameter sweeps.

Table 1. Calculation loads for no-wind testing or travel.

Crane state	Load type	Calculation load
Tyre/truck crane with outriggers extended, or crawler crane	Acting load	1.25PQ + 0.10F
Tyre/truck crane with outriggers retracted	Acting load	1.33PQ + 0.10F
Travel speed ≤ 0.4 m s−1	Acting load	1.33PQ + 0.10F

Crane state	Load type	Calculation load
Travel speed > 0.4 m s−1	Acting load	1.50PQ + 0.10F

Table 2. Load terms for wind-affected operation.

Crane state	Load type	Calculation term	Interpretation
Outriggers extended / crawler	Acting load	1.10PQ	Payload action
Outriggers extended / crawler	Wind	PWII	Working wind
Outriggers extended / crawler	Inertia	PD	Motion inertia
Outriggers retracted	Acting load	1.17PQ	Payload action
Outriggers retracted	Wind	PWII	Working wind
Outriggers retracted	Inertia	PD	Motion inertia
Travel speed ≤ 0.4 m s−1	Acting load	1.17PQ	Payload action
Travel speed ≤ 0.4 m s−1	Wind	PWII	Working wind
Travel speed ≤ 0.4 m s−1	Inertia	PD	Motion inertia
Travel speed > 0.4 m s−1	Acting load	1.33PQ	Payload action
Travel speed > 0.4 m s−1	Wind	PWII	Working wind
Travel speed > 0.4 m s−1	Inertia	PD	Motion inertia

Table 3. Increase coefficients; M6 and γn = 1.20 are used in the baseline calculations.

Mechanism class	M1	M2	M3	M4	M5	M6	M7	M8
Increase coefficient γn	1.00	1.04	1.08	1.12	1.16	1.20	1.25	1.30

Load equations and notation

Equations (1)–(8) define load situations I–III. The P terms denote motor- or brake-related actions; barred terms denote reaction-type actions not balanced by drive-shaft torque. QH and QC represent lifted-mass and moving-crane-component actions, A represents inertia associated with acceleration or braking, f represents friction not already included through transmission efficiency, and W denotes wind.

$$P_{M,\max,I} = \gamma_n \left(P_{QH} + P_{QC} + P_A + P_f\right) \tag{1}$$

$$\overline{P}_{M,\max,I} = \gamma_n \left(\overline{P}_{QG} + \overline{P}_{GC} + \overline{P}_A\right) \tag{2}$$

$$P_{M,\max,II} = \gamma_n \left(P_{QH} + P_{QC} + P_A + P_f + P_{WII}\right) \tag{3}$$

$$P_{M,\max,II} = \gamma_n \left(P_{QH} + P_{QC} + P_A + P_f + 4P_{WI}\right) \tag{4}$$

$$\overline{P}_{M,\max,II} = \gamma_n \left(\overline{P}_{QG} + \overline{P}_{GC} + \overline{P}_A + \overline{P}_{WII}\right) \tag{5}$$

$$\overline{P}_{M,\max,III} = \overline{P}_{MG} + \overline{P}_{WIII} \tag{6}$$

$$P_{M,\max,I,II} = \gamma_n \left(P_{QH} + P_{QC}\right) \tag{7}$$

$$P_{M,\max,III} = 1.6 \left(P_{QH} + P_{QC}\right) \tag{8}$$

Equations (9)–(15) define the wind forces for the seven governing configurations. C is the aerodynamic coefficient, Kh is the height coefficient, pWI and pWIII are working and non-working pressures, and A is the projected area normal to the wind. Force is converted to moment only after multiplication by an explicitly stated effective height.

$$F_1 = CK_h p_{WIII} A \tag{9}$$

$$F_3 = Cp_{WI} A \tag{10}$$

$$F_3 = Cp_{WI} A \tag{11}$$

$$F_9 = Cp_{WI} A \tag{12}$$

$$F_9 = Cp_{WI} A \tag{13}$$

$$F_{12} = Cp_{WI} A \tag{14}$$

$$F_{12} = Cp_{WI} A \tag{15}$$

Governing stability configurations

Figure 3 defines the non-working wind case with C = 1.3, Kh = 1.0, pWIII = 500 N m−2, A = 0.9 m², a 585 N wind resultant and an effective force height of 2.18 m. With a 1000 kg vehicle weight represented as 9800 N and a 0.347 m restoring arm, the stabilising and overturning moments are 3400.6 and 1275.3 N m, respectively.

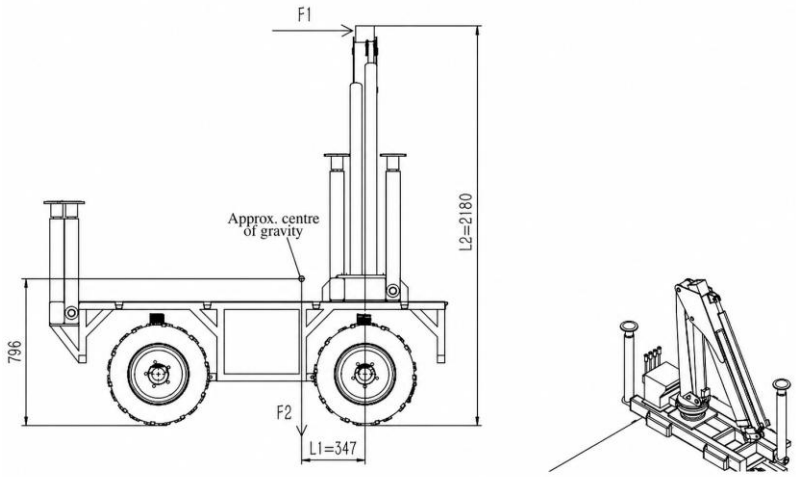


Figure 3. Non-working wind force and corresponding stabilising and overturning lever arms.

Figures 4 and 5 show empty and loaded longitudinal travel at 15°. The empty case uses a 9800 N weight, a projected stabilising arm of 0.1303 m, a 175.5 N working-wind force and a 780 N amplified longitudinal inertia force. The loaded case uses a total 19,600 N weight, a 0.3634 m stabilising arm and a 1560 N inertia force. Both calculations use γn = 1.20. The empty case is much closer to equality because its centre of gravity projects near the downhill tipping line.

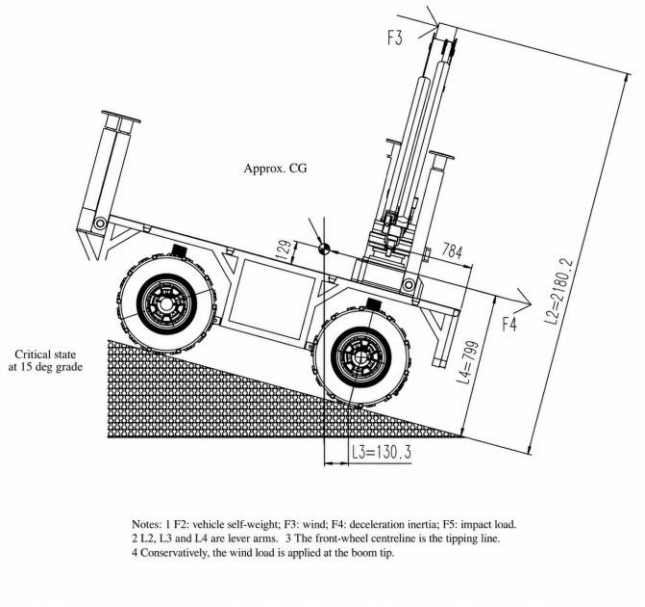


Figure 4. Empty-vehicle longitudinal-slope configuration at 15°.

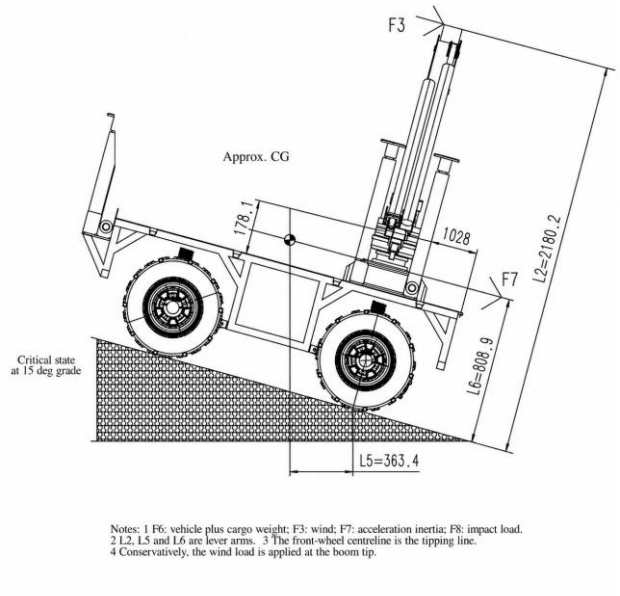


Figure 5. Loaded-vehicle longitudinal-slope configuration at 15°.

Figures 6 and 7 show empty and loaded turning on a 15° cross-slope at a 5 m radius and 3 m s−1 speed. Centrifugal forces are 1800 N for the 1000 kg empty state and 3600 N for the 2000 kg loaded state. The loaded stabilising moment is calculated using the full 19,600 N weight, giving 5001.92 N m.

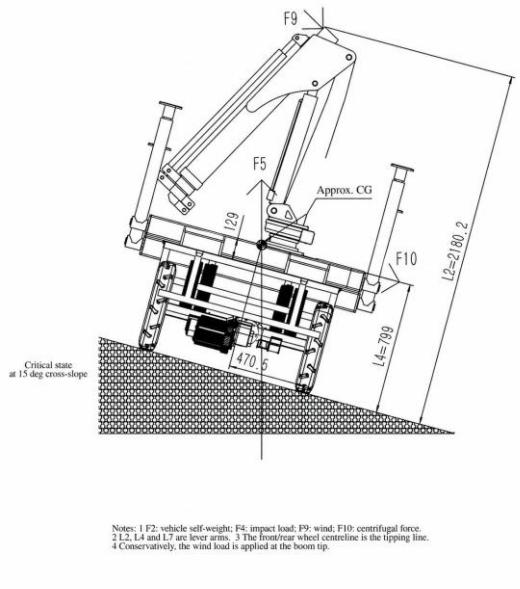


Figure 6. Empty-vehicle lateral-slope turning configuration.

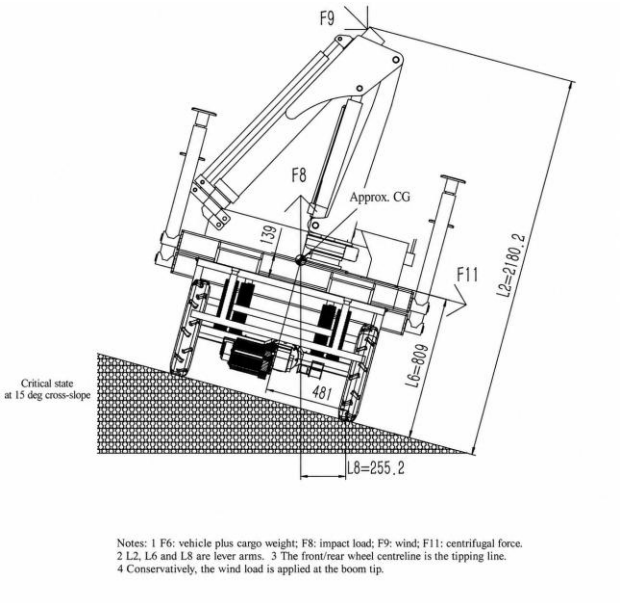


Figure 7. Loaded-vehicle lateral-slope turning configuration.

Figures 8 and 9 define two limiting lifting orientations for a fully extended boom carrying 200 kg. The restoring moments are 3056.816 and 3067.4 N m, the payload lever arms are 0.687 and 0.685 m, and the chassis-boom angles are approximately 85° and 73.5°. A 261.495 N working-wind force is obtained for C = 1.3, pWI = 150 N m−2 and A = 1.341 m². The baseline lifting moment includes this wind action at a 1.5 m effective height, and uncertainty analysis varies the height to quantify its influence.

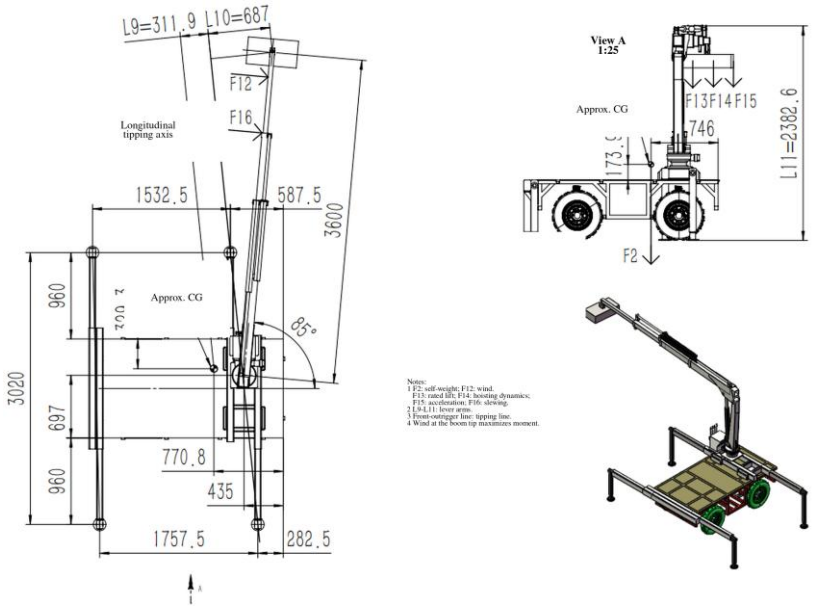


Figure 8. Clockwise limiting lift orientation at approximately 85°.

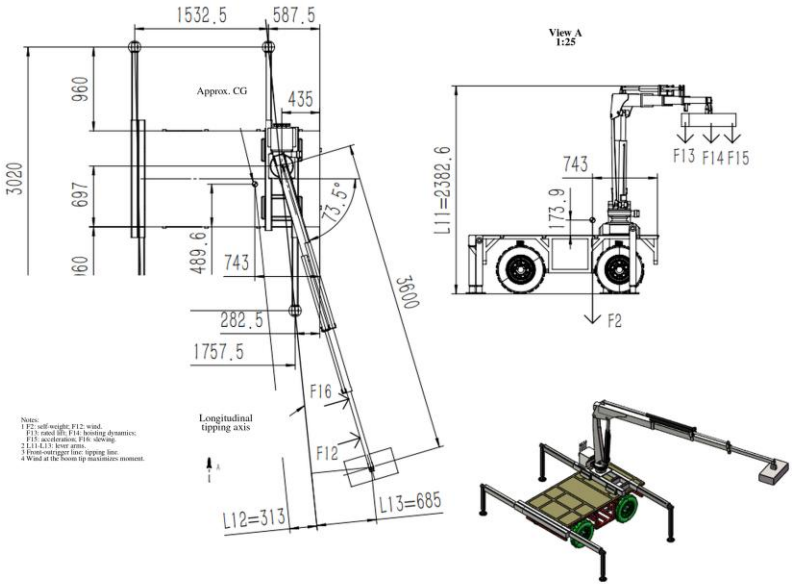


Figure 9. Counter-clockwise limiting lift orientation at approximately 73.5°.

Methods

Evidence boundary and workflow

The analysis uses a deterministic mechanics model followed by fixed-seed uncertainty propagation; no prototype measurements are treated as model inputs. Figure 10 summarises the workflow from geometry and load definition through baseline calculation, boundary sweeps, uncertainty analysis and measurement priorities. All computed quantities are interpreted as screening predictions rather than measured safety performance.

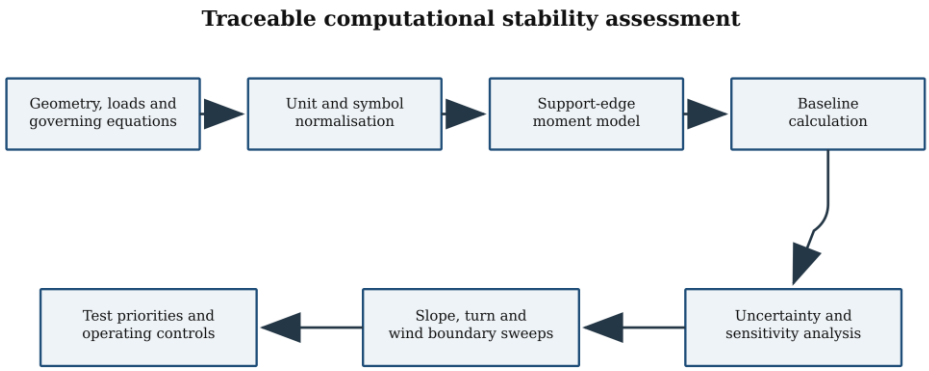


Figure 10. Computational workflow from geometry and load definition to support-edge stability boundaries, uncertainty analysis and operating controls.

Unified support-edge moment model

The stability calculation is written about the governing tipping edge. For longitudinal travel on a slope θ, the projected restoring arm is a cosθ − hG sinθ, where a is the level-ground horizontal distance between the centre of gravity and the tipping line and hG is centre-of-gravity height. Equation (16) converts this lever-arm construction into a continuous slope model. Effective values of a and hG are 0.3493 and 0.800 m for the empty case, and 0.5371 and 0.600 m for the loaded case. These are rigid-body modelling parameters rather than direct scale measurements.

$$M_S(\theta) = mg\,(a\cos\theta - h_G\sin\theta) \tag{16}$$

The longitudinal overturning moment in Eq. (17) combines working wind and amplified acceleration. With φ5 = 2.0, the inertial forces are 780 and 1560 N for empty and loaded travel at 0.39 m s−2. A 2.18 m wind height and the configuration-specific inertia heights define the corresponding moments. The M6 increase coefficient multiplies the combined horizontal action.

$$M_{O,L} = \gamma_n\,(CpAh_W + \phi_5 m a_L h_I) \tag{17}$$

Lateral turning uses the centrifugal resultant in Eq. (18). Equation (19) converts it to overturning moment and adds the working-wind term. The baseline uses 3 m s−1 speed, 5 m turning radius and the specified effective lever arms. The road-tyre friction limit is outside scope; thus, a state predicted stable against rollover can still be unacceptable because of sliding, steering authority or surface failure. Roughness and settlement can change skidding and rollover margins differently [15].

$$F_C = \frac{mv^2}{r} \tag{18}$$

$$M_{O,T} = \gamma_n\,(CpAh_W + F_C h_T) \tag{19}$$

In lifting, the special-load factor 1.6 multiplies the dynamically amplified payload force, as shown in Eq. (20). Wind moment is added independently through Eq. (21). The payload mass is 200 kg, φ2 = 1.202, the two payload arms are 0.687 and 0.685 m, and the baseline wind-force height is 1.50 m. Wind height is varied from 1.20 to 1.80 m in uncertainty propagation because the pressure-centre location has not been measured. Ground settlement, outrigger compliance, chassis torsion, load swing and hydraulic drift are not represented.

$$M_{O,Q} = 1.6\,\phi_2 m_Q g\, l_Q \tag{20}$$

$$M_{O,W} = CpAh_W \tag{21}$$

Stability measures and boundary calculations

Two equivalent measures are reported. The stability factor K in Eq. (22) is the ratio of stabilising to overturning moment; K = 1 denotes moment equality. The normalised reserve R in Eq. (23) expresses the remaining moment as a fraction of stabilising moment. Positive R is stable within the rigid-body model, zero is the calculated tipping boundary and negative R is unstable. A screening line K = 1.10 is shown in figures to identify cases with only a small deterministic reserve; it is an analytical alert level rather than a statutory factor.

$$K = \frac{M_S}{M_O} \tag{22}$$

$$R = \frac{M_S - M_O}{M_S} = 1 - \frac{1}{K} \tag{23}$$

The critical turn speed in Eq. (24) follows by setting the lateral moment equality and solving for v. Similar root finding is used for critical slope. For lift wind exposure, the critical area follows from Acrit = (MS − MOQ)/(Cp hW). These closed-form or one-dimensional boundaries are more informative than an isolated statement that one tested state was stable, because they show the distance from the boundary and the variable responsible for crossing it.

$$v_{\mathrm{cr}} = \sqrt{\frac{r\left(M_S/\gamma_n - CpAh_W\right)}{mh_T}} \tag{24}$$

Uncertainty propagation and sensitivity

Fixed-seed Monte Carlo propagation used N = 10,000 evaluations per state. Mass scale was normally distributed around 1.00 with a 0.03 standard deviation and bounded to 0.90–1.10. Geometry scale used a 0.035 standard deviation and bounds of 0.88–1.12. The increase coefficient was uniform over 1.15–1.25; working pressure over 100–200 N m−2; non-working pressure over 400–600 N m−2; slope over 13–17°; longitudinal acceleration over 0.30–0.48 m s−2; turning speed over 2.5–3.5 m s−1; and radius over 4.5–5.5 m. Lift area varied from 1.20 to 1.50 m², wind height from 1.20 to 1.80 m and φ2 from 1.15 to 1.25. These ranges are engineering screening assumptions, not fitted site distributions.

Equation (25) estimates the fraction of model evaluations with negative reserve. It is intentionally described as model P(R < 0), not an accident probability. Rank correlation screens monotonic sensitivity for the weakest travel and lift cases. Because correlation does not prove causality and periodic or interacting effects can be understated, the coefficients are used to prioritise measurement rather than assign formal importance weights.

$$\widehat{P}_f = \frac{1}{N}\sum_{k=1}^{N} \mathbf{1}(R_k < 0) \tag{25}$$

Table 4. Baseline parameter values and explicit uncertainty assumptions.

Quantity	Baseline / range	Evidence class	Role
Empty / loaded travel mass	1000 / 2000 kg	Specified value	Gravity and inertia
Working / non-working wind pressure	150 / 500 N m−2	Specified value	Wind resultant

Quantity	Baseline / range	Evidence class	Role
Projected area: travel / lift	0.3–0.9 / 1.341 m²	Specified value	Wind resultant
Increase coefficient γn	1.20; range 1.15–1.25	Specified value + uncertainty range	Combined travel actions
Dynamic lifting coefficient φ2	1.202; range 1.15–1.25	Specified value + uncertainty range	Payload action
Slope	15°; range 13–17°	Specified value + uncertainty range	Gravity projection
Turn speed / radius	3 m s−1 / 5 m	Specified value	Centrifugal action
Lift wind-force height	1.50 m; range 1.20–1.80 m	Explicit assumption	Wind moment
Monte Carlo sample count / seed	10,000 per state / 20260809	Reproducibility choice	Uncertainty screening

Results

Deterministic state results

Table 5 and Fig. 11 compare the seven baseline states. The non-working wind case has K = 2.67. Empty longitudinal travel is the closest travel state to moment equality: MS = 1276.9 N m, MO = 1207.0 N m, K = 1.058 and R = 0.055. Loaded longitudinal travel has K = 3.61 because the specified cargo distribution shifts the projected centre of gravity away from the downhill tipping line. This result should not be generalised to arbitrary cargo placement; it applies only to the 0.3634 m projected lever arm.

Empty and loaded lateral turning have K = 1.29 and 1.25. The two lift orientations are substantially more critical when working-wind moment is included. At the baseline 1.50 m wind height, K is 1.025 at 85° and 1.031 at 73.5°; without wind, the factors would be approximately 1.18–1.19. The lifting states therefore remain positive in the deterministic calculation but have only a small reserve that depends strongly on the unmeasured pressure-centre height.

Table 5. Baseline moments and stability measures. Lift cases include working-wind moment at hW = 1.50 m.

State	MS (N m)	MO (N m)	K	R
Non-working wind	3400.6	1275.3	2.667	0.625
Empty longitudinal travel	1277.6	1207.0	1.059	0.055
Loaded longitudinal travel	7124.0	1973.6	3.610	0.723
Empty lateral turn	2427.5	1878.9	1.292	0.226
Loaded lateral turn	5000.8	3993.5	1.252	0.201
Lift at 85°	3056.8	2981.9	1.025	0.025
Lift at 73.5°	3067.4	2974.3	1.031	0.030

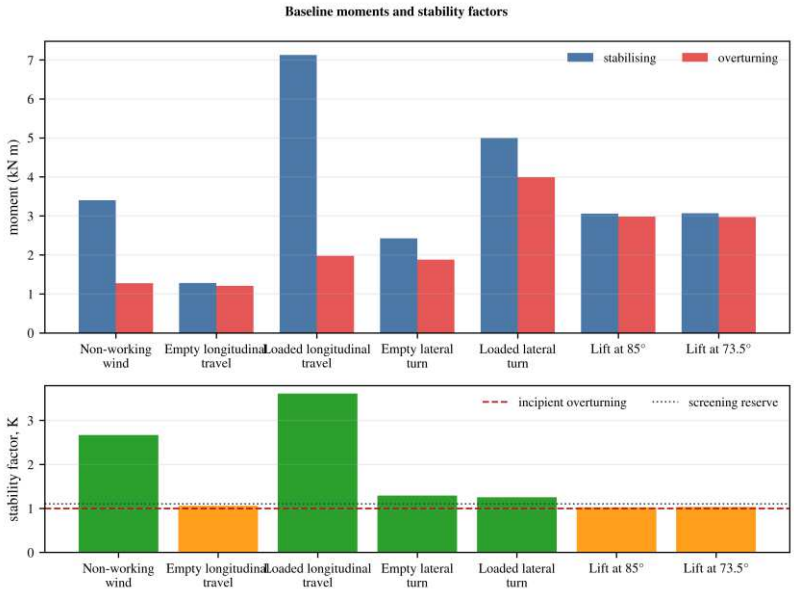


Figure 11. Baseline stabilising and overturning moments and corresponding stability factors. K = 1 is moment equality; K = 1.10 is a screening alert line rather than a code-prescribed factor.

Longitudinal slope boundary

Figure 12 evaluates longitudinal travel over a continuous 0–25° slope range. The empty-state restoring moment falls rapidly because its level-ground centre-of-gravity distance is small relative to height. Under the specified wind and acceleration actions, the first model point with $R \leq 0$ occurs near 15.5°. Numerical resolution is 0.1°, so the result should be interpreted as approximately 15.5°, not an exact certified angle. A 15° operating point therefore provides only about half a degree of deterministic angular separation in this idealised case.

The loaded-state curve remains positive throughout the plotted range and crosses zero beyond it. This favourable result follows from the specified loaded lever arm and cannot be used to argue that cargo always improves stability. Cargo placed high, laterally offset or able to shift would increase hG or reduce a. The model consequently supports a rule based on measured load distribution, not a blanket permission to carry mass as counterweight. Recent tractor research similarly shows that overall mass alone does not determine rollover resistance when structure and mass distribution change [12,13].

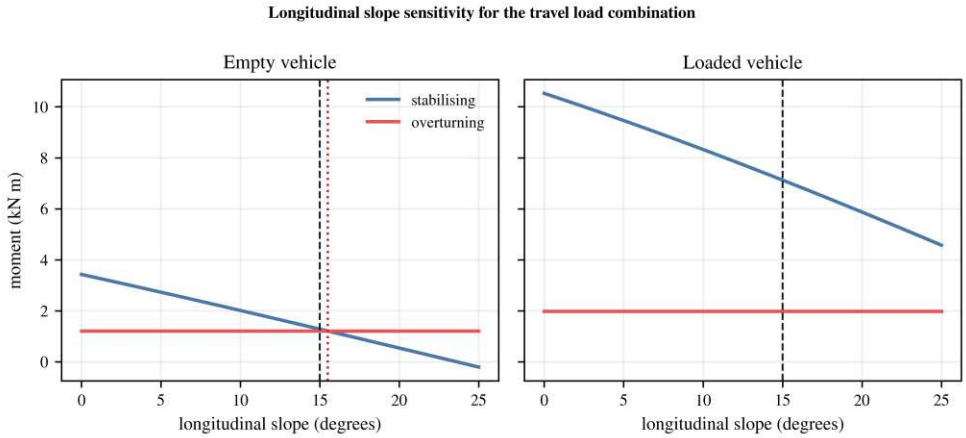


Figure 12. Longitudinal stabilising and overturning moments versus slope. The dashed line marks the 15° operating point; the dotted line marks the first calculated moment equality where present.

Lateral turning envelope

Figure 13 maps the normalised reserve R over 0.5–4.5 m s−1 and turning radii of 3–8 m at a 15° cross-slope. At r = 5 m, moment equality occurs at approximately 3.44 m s−1 for the empty model and 3.38 m s−1 for the

loaded model. An operating point of 3 m s−1 is therefore conservative relative to calculated overturning, but the margin is moderate rather than large. A tighter turn raises centrifugal force in inverse proportion to radius, so the same speed cannot be transferred to a 3 m turn.

The heatmaps also clarify why speed control should be continuous. Centrifugal action varies with v^2; an increase from 3.0 to 3.5 m s−1 raises this component by approximately 36%, not 17%. Operator instructions stated only as a nominal maximum may be difficult to enforce on downhill or irregular tracks. A practical system should combine measured speed, steering-derived radius and chassis roll angle, issue a warning before the zero-reserve contour and prevent simultaneous high speed and tight steering. The analytical result is consistent with multidimensional rollover studies in which velocity and centre-of-gravity effects interact [14].

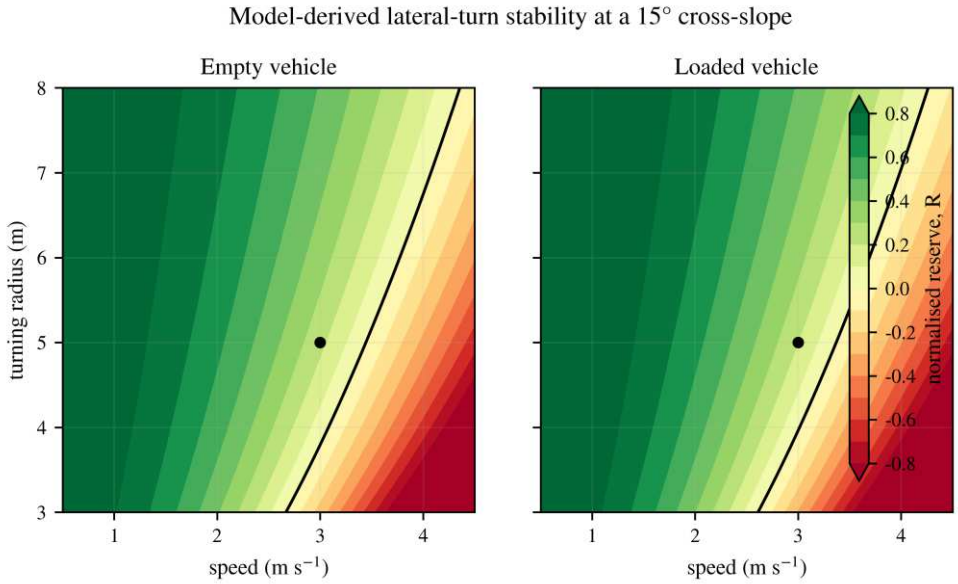


Figure 13. Normalised reserve for empty and loaded turning at a 15° cross-slope. The black contour is R = 0 and the black point denotes 3 m s−1 at a 5 m radius.

Wind pressure, projected area and lifting margin

Figure 14 demonstrates that projected area cannot be treated as an independent stop criterion. At the baseline pressure of 150 N m−2 and a 1.50 m wind-force height, the critical areas are approximately 1.65 m² at 85° and 1.66 m² at 73.5°. The 1.341 m² operating area lies inside the positive region but close to the zero contour. If pressure rises, the critical area falls in inverse proportion. If the effective height increases to 2.18 m, the same 1.341 m² lift state crosses the calculated boundary at a substantially lower pressure. A defensible wind limit must therefore specify pressure, projected area and force height together.

Operationally, the relevant observable is wind moment or a validated configuration-specific wind limit. Projected boom area can be obtained from geometry, but a suspended tower member or sheet-like load may contribute a much larger and rapidly changing area. Wind speed should be measured with an anemometer located away from obstruction and converted to the pressure convention used in the load chart. Gust and averaging rules must be specified. Recent analytical crane studies show substantial directional variation in critical wind condition [9], and wind-aware planning treats meteorology as a configuration input [2].

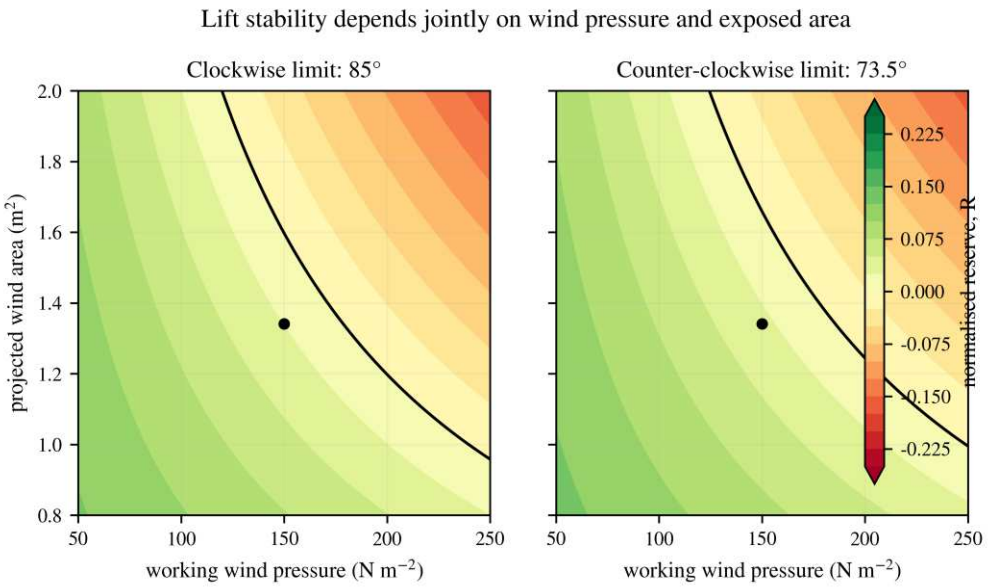


Figure 14. Lift reserve versus working wind pressure and projected area at the two limiting orientations. The black point denotes 150 N m^{-2} and 1.341 m²; calculations use a 1.50 m effective wind height.

Deterministic perturbations and uncertainty propagation

Figure 15 compares one-at-a-time changes around each baseline. Wind pressure mainly affects non-working wind and lifting. An additional 0.5° slope most strongly reduces the empty longitudinal reserve. Increasing speed or reducing radius dominates turning. Wind-force height affects the lift states but not the travel equations. The matrix is intentionally sparse: a blank or near-zero cell means that the selected perturbation is absent from that state equation, not that the physical quantity can never matter.

Fixed-seed uncertainty propagation in Fig. 16 changes the interpretation of the deterministic pass/fail result. Non-working wind and loaded longitudinal travel remain positive for almost all selected samples. The empty longitudinal case spans both sides of R = 0 because the baseline condition has only 5.5% normalised reserve. The two turning cases also develop negative tails when high speed, small radius, steep slope and geometry uncertainty coincide. Both lift cases have distributions centred near zero because uncertainty in restoring moment, φ2, pressure, area and wind height is comparable with the baseline margin.

These model fractions are not real-world accident probabilities. They depend on deliberately broad uniform or bounded distributions and omit correlations. Their value is diagnostic: a design that changes classification under small reasonable parameter changes requires better measurement or more physical reserve. Figure 17 confirms that empty longitudinal stability is controlled primarily by slope, effective geometry and acceleration, whereas lift stability is controlled by restoring moment, φ2, wind height, pressure and area. The ordering supports direct measurement of centre of gravity, support geometry and pressure centre before collecting less influential detail.

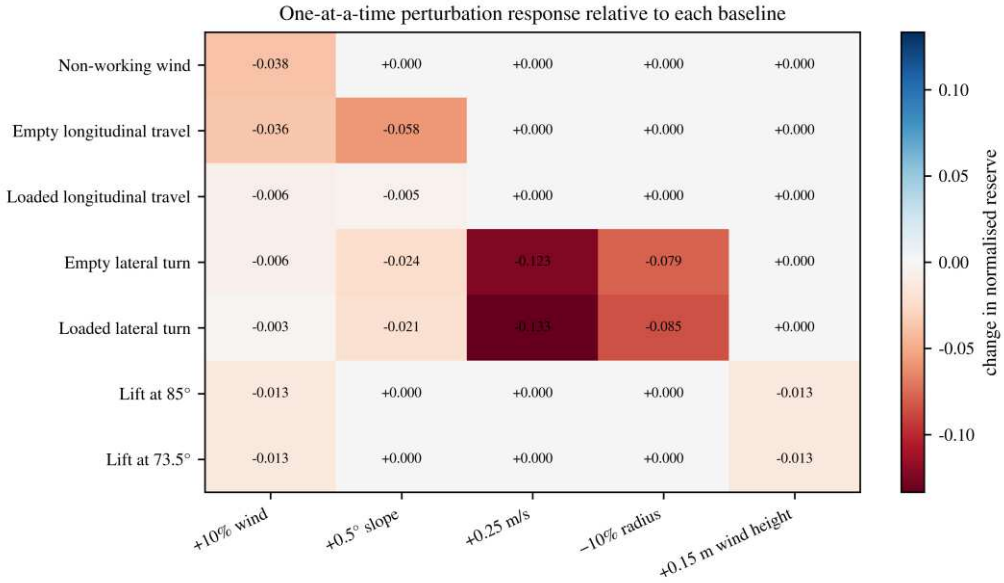


Figure 15. One-at-a-time change in normalised reserve for five engineering perturbations. Values are changes from each state-specific baseline, not absolute reserve.

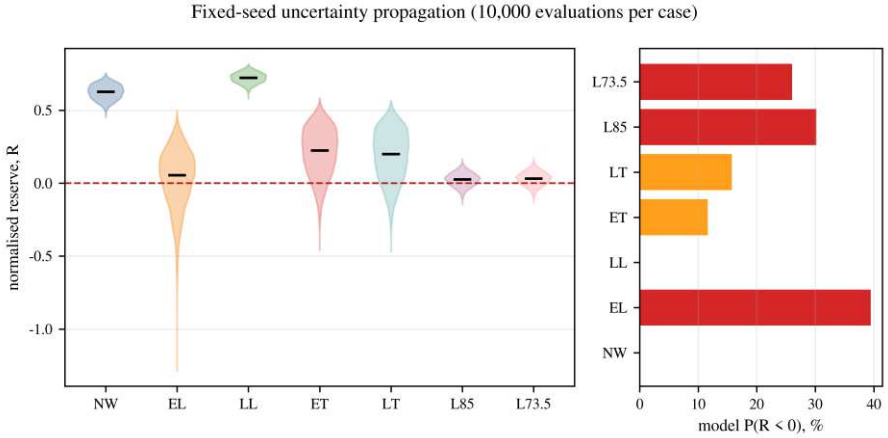


Figure 16. Fixed-seed uncertainty distributions and model fraction with R < 0 for seven governing states (10,000 evaluations per state). NW, EL, LL, ET, LT, L85 and L73.5 denote non-working wind, empty/loaded longitudinal, empty/loaded turning and the two lift orientations.

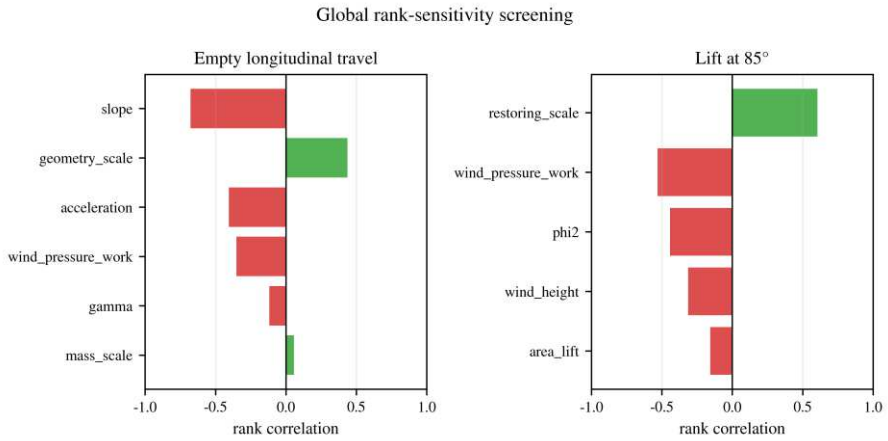


Figure 17. Rank-correlation sensitivity for the weakest travel and lift baselines. Correlations rank measurement priorities; they do not establish causal importance or replace interaction analysis.

Table 6. Fixed-seed uncertainty results. Fractions are conditional model outputs, not field failure probabilities.

State	Median R	5th–95th percentile	Model P(R < 0)

State	Median R	5th–95th percentile	Model P(R < 0)
Non-working wind	0.626	0.538 to 0.704	0.0%
Empty longitudinal travel	0.055	-0.342 to 0.309	39.5%
Loaded longitudinal travel	0.722	0.660 to 0.779	0.0%
Empty lateral turn	0.224	-0.083 to 0.450	11.6%
Loaded lateral turn	0.200	-0.114 to 0.437	15.7%
Lift at 85°	0.026	-0.054 to 0.099	30.2%
Lift at 73.5°	0.032	-0.048 to 0.104	26.0%

Table 7. Model-derived operating boundaries and corresponding validation requirements.

Boundary	Model-derived value	Interpretation	Required validation
Empty longitudinal slope	≈15.5° at moment equality	Supports a conservative 15° operating limit	Tilt/platform test with wheel reactions
Empty turn at r = 5 m	≈3.44 m s−1	3 m s−1 leaves moderate reserve	Instrumented constant-radius turn
Loaded turn at r = 5 m	≈3.38 m s−1	Loaded state governs slightly	Repeat with representative cargo distribution
Lift area at 85°, p = 150 N m−2	≈1.65 m² for hW = 1.50 m	Area limit depends on pressure and height	Wind-force/pressure-centre test
Lift area at 73.5°, p = 150 N m−2	≈1.66 m² for hW = 1.50 m	Similar small baseline reserve	Reaction measurement across slew sector

Discussion

Interpretation of operating boundaries

The 15° longitudinal operating point is a conservative boundary for the empty model geometry, but it is not a universal gradeability rating. The calculation assumes a rigid chassis, fixed centre of gravity, firm support and constant acceleration. A local bump, braking transient or cargo shift can reduce the effective lever arm without changing the average road grade. Road-level estimation and direct inclination sensing should therefore accompany the written limit [7].

The 3 m s−1 turning point is supported for a 5 m radius and a 15° cross-slope. It should be expressed as a speed–radius–slope envelope rather than a single number. Because centrifugal moment varies with v^2/r, electronic speed limitation can be implemented from measured wheel speed and steering geometry. Field manoeuvres may contain tighter transient curvature, so wheel unloading or outrigger reaction sensing should complement the geometric estimate [4].

The boom-angle boundaries require more caution. Figures 8 and 9 define two static configurations but do not represent the complete 360° slew envelope. The 85° and 73.5° states are therefore treated as validation points rather than universal safe-sector limits. The governing edge can change with azimuth, support extension, chassis attitude and payload swing. Rotary-crane assessment should sample the complete slew range [1], and a future load-moment limiter should use measured boom length, angle, slew position, payload and support state.

The 1.34 m² wind-area statement changes most substantially. Area is one factor in wind force and cannot alone define a safe limit. The pressure, aerodynamic coefficient, force height, payload area and orientation must accompany it. The baseline result remains positive for the assumed 1.50 m height, but the uncertainty distribution shows limited robustness. A configuration-specific wind-speed limit is more defensible than a universal projected-area cutoff.

Engineering and safety implications

The analysis suggests a layered protection strategy. First, passive geometry should provide adequate support before software intervention. Longitudinal support span is especially important because rear outriggers may increase lateral width without increasing the distance to a front or rear tipping line. Increasing only lateral span would improve the turning and side-lift states while leaving empty longitudinal travel nearly unchanged. Variable-span outrigger calculations can quantify individual support reactions and detect partial deployment [23].

Second, travel and lifting modes should be interlocked. Travel should require the boom to be stowed within a validated envelope and the outriggers retracted and secured. Lifting should require the vehicle to be stationary, brakes applied, outriggers fully deployed, support pads seated and platform inclination within limit. The system should not infer deployment solely from a hydraulic command; position or reaction sensors should confirm that the support state used by the calculation exists physically. Coordinated levelling control may reduce attitude error [8], but it cannot compensate for soil bearing failure.

Third, the load chart should be multidimensional. A nominal 200 kg capacity is incomplete without radius, boom angle, slew sector, slope, wind and support condition. Digital-twin lift planning demonstrates how spatial and capacity constraints can be evaluated before execution [11]. For the compact carrier, a simpler embedded lookup table could provide the same principle. Conservative interpolation should be used between validated test points, and any missing or implausible sensor input should default to a safer restricted state.

Fourth, safety management must extend beyond mechanics. Knowledge-based assessment identifies planning and supervision as interacting parts of crane safety [19]. Evolutionary-game analysis shows that organisational incentives influence compliance with tower-crane supervision [20], while Bayesian-network analysis in Scientific Reports demonstrates coupling among human, machine, management and environmental factors [21]. Scenario-based crane-accident assessment likewise supports integrated evaluation instead of single-cause reasoning [22]. For the present machine, operator training, route inspection, wind monitoring, exclusion zones, maintenance and documented pre-use checks are therefore necessary even if the moment calculation passes.

Fifth, loose cargo should not be credited as certified counterweight. The favourable loaded longitudinal result depends on the specified cargo centre of gravity. Cargo may shift, be removed without updating the calculation or overload local deck structure. If ballast is required, it should be a designed, restrained and sensed component included in structural and stability validation. Otherwise, the operating envelope should use the minimum credible stabilising mass.

Conclusions

This study presents a traceable computational analysis of a compact transport vehicle-mounted crane boom. Nine engineering figures, three load tables and fifteen numbered equations define the model. The equations use consistent notation and moment units, the loaded lateral state uses the full vehicle-plus-cargo weight, and working wind is included explicitly in the lifting cases.

The analysis shows that 15° longitudinal travel and 3 m s−1 turning at a 5 m radius are conservative operating points for the specified geometry, but their deterministic reserves are modest in the governing cases. The lifting configurations pass only narrowly after inclusion of baseline wind moment. Projected area alone is not a universal wind stop criterion; pressure and effective force height must be specified. Fixed-seed uncertainty propagation identifies the empty longitudinal and two limiting lift states as priorities for physical validation.

The numerical outputs are model-derived rather than measured. Before field deployment, the complete mass distribution, support reactions, ground bearing, critical slope, turning response, slew-sector load chart and wind pressure centre must be measured. A validated load-moment limiter should combine support state, inclination, boom geometry, payload, speed, radius and wind rather than rely on one nominal capacity or one isolated threshold.

Author contributions

W.D. and Q.Z. conceived the engineering problem. W.D., Q.Z. and Y.D. compiled the design and stability calculations. F.Z. and Y.W. reviewed construction-operability requirements. H.C. reviewed cost and implementation constraints. All authors reviewed the analytical framework and approved the manuscript. The final CRediT roles and corresponding author must be confirmed before submission.

Funding

This work was supported by the State Grid Jiangsu Electric Power Co., Ltd. science and technology project “Development of an autonomous material transport and loading vehicle for transmission-line construction” (HYS22Z10040).

Competing interests

The authors declare no competing interests. This statement should be reconfirmed by all authors before submission.

Data availability

All data generated or analysed during this study are included in this published article.

References

1. Kwiatoń, P., Cekus, D. & Waryś, P. Computer-aided rotary crane stability assessment. Automation in Construction 162, 105370 (2024). https://doi.org/10.1016/j.autcon.2024.105370
2. Hebiba, A. M., Bouferguene, A., Moon, S. & Han, S. Wind-wise automated stability analysis for selection of tower crane and location. Journal of Construction Engineering and Management 148, 04022127 (2022). https://doi.org/10.1061/(ASCE)CO.1943-7862.0002377
3. Song, J. & Sharf, I. Stability-constrained mobile manipulation planning on rough terrain. Robotica 40, 4090–4119 (2022). https://doi.org/10.1017/S0263574722000777
4. Petrović, G. R. & Mattila, J. Analytic solutions for wheeled mobile manipulator supporting forces. IEEE Access 10, 43235–43255 (2022). https://doi.org/10.1109/ACCESS.2022.3169766
5. Song, T., Yang, H., Guo, S., Cui, G. & Yan, Z. Configuration selection for tip-over stability of a modular reconfigurable mobile manipulator under various application situations. Robotica 41, 1066–1085 (2023). https://doi.org/10.1017/S0263574722001424
6. Kacalak, W., Budniak, Z. & Majewski, M. Modelling and analysis of the positioning accuracy in the loading systems of mobile cranes. Materials 15, 8426 (2022). https://doi.org/10.3390/ma15238426
7. Wang, G., Qu, W. & Chen, C. A road level identification method for all-terrain crane based on support vector machine. Measurement 187, 110319 (2022). https://doi.org/10.1016/j.measurement.2021.110319
8. Xu, F., Hu, H., Feng, S. & Zhou, C. Synchronous leveling control method of crane vehicle platform based on position–force coordination. Actuators 14, 441 (2025). https://doi.org/10.3390/act14090441
9. Augustyn, M. & Barski, M. Numerical and analytical determination of the critical wind speed causing the overturning of the top-slewing tower crane. Applied Sciences 15, 4683 (2025). https://doi.org/10.3390/app15094683
10. Cekus, D. & Kwiatoń, P. Stability analysis of mobile crane during wind induced load sway. In Perspectives in Dynamical Systems I—Applications, 145–160 (Springer, 2024). https://doi.org/10.1007/978-3-031-56492-5_11
11. Jang, D.-H., Roh, G.-T., Jeon, C.-H. & Shim, C.-S. Simulation-based optimization of crane lifting position and capacity using a construction digital twin for prefabricated bridge deck assembly. Buildings 15, 475 (2025). https://doi.org/10.3390/buildings15030475
12. Wang, L. et al. Advances in tractor rollover and stability control: implications for off-road driving safety. Computers and Electronics in Agriculture 226, 109483 (2024). https://doi.org/10.1016/j.compag.2024.109483
13. Belloni, M., Vignati, M. & Sabbioni, E. Analysing the effect of chassis torsional flexibility on the rollover threshold of a multi-purpose agricultural vehicle. Vehicles 6, 415–432 (2024). https://doi.org/10.3390/vehicles6010018
14. Nguyen, T. A. Assessing the dependence of vehicle rollover on many factors based on new 4D graphs. PLoS ONE 18, e0284018 (2023). https://doi.org/10.1371/journal.pone.0284018
15. Sun, L., Chen, L., Yin, Y., Tian, Y. & Zhang, X. Risk assessment of rollover and skidding due to pavement roughness and differential settlement for enhancing transportation safety. Journal of Advanced Transportation 2021, 7244283 (2021). https://doi.org/10.1155/2021/7244283
16. Tao, Y., Liu, H., Song, Y., Deng, C., Wang, B. & Zheng, P. Dynamic tip-over avoidance method for mobile manipulators based on the extended zero-moment point algorithm for human–robot collaboration. Journal of Computing and Information Science in Engineering 25, 051003 (2025). https://doi.org/10.1115/1.4067523
17. Toledo Fuentes, A., Kempf, F., Kipfmüller, M., Bergmann, T. & Prieto, M. J. Tip-over detection and avoidance algorithms as stabilization strategy for small-footprint and lightweight mobile manipulators. Machines 11, 44 (2023). https://doi.org/10.3390/machines11010044
18. Cheng, C., Zhang, H., Peng, H., Zhou, Z., Chen, B., Zeng, Z. & Lu, H. Stability control for end effect of mobile manipulator in uneven terrain based on active disturbance rejection control. Assembly Automation 41, 369–383 (2021). https://doi.org/10.1108/AA-10-2020-0157
19. Sadeghi, H. & Zhang, X. Towards safer tower crane operations: an innovative knowledge-based decision support system for automated safety risk assessment. Journal of Safety Research 90, 272–294 (2024). https://doi.org/10.1016/j.jsr.2024.05.011
20. Chen, Y., Zeng, Q., Zheng, X., Shao, B. & Jin, L. Safety supervision of tower crane operation on construction sites: an evolutionary game analysis. Safety Science 152, 105578 (2022). https://doi.org/10.1016/j.ssci.2021.105578
21. Wu, B.-J., Jin, L.-H., Zheng, X.-Z. & Chen, S. Coupling analysis of crane accident risks based on Bayesian network and the N-K model. Scientific Reports 14, 1133 (2024). https://doi.org/10.1038/s41598-024-51425-9
22. He, W., Lin, Z., Li, W., Wong, C. J., Kong, D. & Loh, W. E. The comprehensive safety assessment method for complex construction crane accidents based on scenario analysis: a case study of crane accidents. Computers & Industrial Engineering 199, 110716 (2025). https://doi.org/10.1016/j.cie.2024.110716
23. Chang, Z., Zhang, Z., Yang, M., Deng, Q. & Wu, J. Inverse seeking method to find the force of the variable span outrigger of truck crane based on analytic method and its algorithm realization. In Advances in Mechanical Design, 47–61 (Springer, 2024). https://doi.org/10.1007/978-981-97-0922-9_4

24. Carabin, G., Karaca, M. & Mazzetto, F. Preliminary results of extensive tractor rollover stability tests using a tilting-rotating rig. Biosystems Engineering 254, 104146 (2025). https://doi.org/10.1016/j.biosystemseng.2025.104146
25. Tran, D. H., Nguyen, S. N. & Nguyen, X. C. Modeling and investigating the dynamics of hydraulic telescopic truck cranes. Advances in Science and Technology Research Journal 18, 125–138 (2024). https://doi.org/10.12913/22998624/190266